2-1-2024

Analysis of the outer retinal bands in ABCA4 and PRPH2-associated retinopathy using OCT

Rachael C. Heath Jeffery

Johnny Lo
Edith Cowan University

Jennifer A. Thompson

Tina M. Lamey

Terri L. McLaren

See next page for additional authors

10.1016/j.oret.2023.05.010
Jeffery, R. C. H., Lo, J., Thompson, J. A., Lamey, T. M., McLaren, T. L., De Roach, J. N., . . . Chen, F. K. (2024). Analysis of the outer retinal bands in ABCA4 and PRPH2-associated retinopathy using OCT. Ophthalmology Retina, 8(2), 174-183. https://doi.org/10.1016/j.oret.2023.05.010

AMERICAN ACADEMY OF OPHTHALMOLOGY®

Analysis of the Outer Retinal Bands in *ABCA4* and *PRPH2*-Associated Retinopathy using OCT

Rachael C. Heath Jeffery, MChD, MPH,[1,2,3] Johnny Lo, PhD,[4] Jennifer A. Thompson, PhD,[5] Tina M. Lamey, PhD,[1,5] Terri L. McLaren, BSc,[1,5] John N. De Roach, PhD,[1,5] Lauren N. Ayton, PhD,[6,7,8] Andrea L. Vincent, MBChB, MD,[9,10] Abhishek Sharma, MBBS, DPhil,[11] Fred K. Chen, MBBS, PhD[1,2,3,5,7,8]

Purpose: To evaluate the outer retinal bands using OCT in *ABCA4*- and *PRPH2*-associated retinopathy and develop a novel imaging biomarker to differentiate between these 2 genotypes.

Design: Multicenter case-control study.

Participants: Patients with a clinical and genetic diagnosis of *ABCA4*- or *PRPH2*-associated retinopathy and an age-matched control group.

Methods: Macular OCT was used to measure the thickness of the outer retinal bands 2 and 4 by 2 independent examiners at 4 retinal loci.

Main Outcome Measures: Outcome measures included the thicknesses of band 2, band 4, and the band 2/band 4 ratio. Linear mixed modeling was used to make comparisons across the 3 groups. Receiver operating characteristic (ROC) analysis determined the optimal cutoff for the band 2/band 4 ratio to distinguish *PRPH2*- from *ABCA4*-associated retinopathy.

Results: We included 45 patients with *ABCA4* variants, 45 patients with *PRPH2* variants, and 45 healthy controls. Band 2 was significantly thicker in patients with *PRPH2* compared with *ABCA4* (21.4 vs. 15.9 μm, $P < 0.001$) variants, whereas band 4 was thicker in patients with *ABCA4* variants than those with *PRPH2* variants (27.5 vs. 21.7 μm, $P < 0.001$). Similarly, the band 2/band 4 ratio was significantly different (1.0 vs. 0.6 for *PRPH2* vs. *ABCA4*, $P < 0.001$). The area under the ROC curve was 0.87 for either band 2 (> 18.58 μm) or band 4 (< 26.17 μm) alone and 0.99 (95% confidence interval: 0.97−0.99) for the band 2/band 4 ratio with a cutoff threshold of 0.79, providing 100% specificity.

Conclusions: We report an altered outer retinal band profile whereby the band 2/band 4 ratio was able to discriminate between *PRPH2*- and *ABCA4*-associated retinopathy. This may have future clinic utility in predicting the genotype and provide further insight into the anatomic correlate of band 2.

Financial Disclosure(s): Proprietary or commercial disclosure may be found in the Footnotes and Disclosures at the end of this article. *Ophthalmology Retina 2024;8:174-183*

Supplemental material available at www.ophthalmologyretina.org.

Advancements in OCT technology have revealed novel imaging biomarkers to facilitate the diagnosis and monitoring of inherited retinal diseases (IRDs).[1,2] *In vivo* visualization of the integrity of the 4 hyperreflective outer retinal bands has enhanced our ability to compare IRDs with a similar phenotype, such as fundus flavimaculatus because of mutations in *ABCA4* or *PRPH2*.[3] Considering that *PRPH2* mutations can be nonpenetrant[4] and *ABCA4* pedigrees may show pseudodominant inheritance,[5] these 2 diseases may not be easily differentiated based on family history, clinical examination, or even quantitative fundus autofluorescence (qAF).[6] We hypothesize differences in the outer retinal bands may distinguish *PRPH2*- from *ABCA4*-associated retinopathy.

Spaide and Curcio[7] provided histologic evidence for the colocalization of the second outer retinal band (band 2) with the mitochondrial rich ellipsoid zone (EZ) of the inner segment (IS). Anatomic correlates of bands 3 and 4 have been debated (Fig 1).[8,9] The 2014 International Nomenclature for OCT panel[10] discussed evidence from electron microscopy[11] in which band 3 represented the contact cylinder or interdigitation zone between the outer segment (OS) and the retinal pigment epithelium (RPE) microvilli whereas band 4 represented the RPE/Bruch complex. Later, Cuenca et al[12] described bands 3 and 4 as the phagosome and mitochondria zones of the RPE, respectively, using anti-cellular retinaldehyde−binding protein (CRALBP) antibody-staining. Bloom and Singal

https://doi.org/10.1016/j.oret.2023.05.010
ISSN 2468-6530/23

et al[13] used central serous chorioretinopathy as a disease model to illustrate that both bands 3 and 4 cannot simultaneously reside within the RPE because these bands separate during active central serous chorioretinopathy. Similarly, we have shown increased visibility and separation of band 3 from band 4 after the use of fibroblast growth factor receptor inhibitors.[14] Hence, detailed OCT investigation of other disease models may provide further insight into the composition of these outer retinal bands. Electron microscopy of *PRPH2* mutant mice showed disorganized OS,[15] which is supported by studies from human retinal tissue.[16] In contrast, *ABCA4* mutant mice exhibited an accumulation of RPE lipofuscin granules with increased vacuolation and phagosomes.[17] Hence, both these diseases may uniquely alter the profile of bands 2 to 4 and provide insights into their origins.

The purpose of this study was to compare the outer retinal bands in patients with *ABCA4*- and *PRPH2*-associated retinopathy. The thickness of bands 2 and 4 were measured to shed light on what substructures they may represent with comparisons to healthy controls. We aimed to develop a novel imaging biomarker to segregate these 2 IRDs.

Methods

Study Design

This was an international multicenter case-control study. The study was performed in accordance with the Declaration of Helsinki and approved by the Institutional Ethics Committees (University of Western Australia, Authorization RA/4/1/7916, RA/4/20/5454, RA/4/1/8932, and 2021/ET000151 and Sir Charles Gairdner Hospital Human Research Ethics Committee, Authorization RGS04985, the Royal Victorian Eye and Ear Hospital Human Research Ethics Committee 19/1443H, New Zealand Ministry of Health NTX/08/12/123, and Auckland District Health Board A+4290). Informed written consent was obtained from patients and controls before enrollment. Participants were recruited from October 2013 to December 2022 from the following centers: Lions Eye Institute (Perth, Australia), Centre for Eye Research Australia (Melbourne, Australia),[18] Queensland Eye Institute (Brisbane, Australia), and Auckland District Health Board (Auckland, New Zealand).

Patient Population

Patients with a clinical diagnosis of Stargardt disease and biallelic pathogenic or likely pathogenic *ABCA4* variants or a diagnosis of *PRPH2*-retinopathy supported by a heterozygous pathogenic or likely pathogenic variant in *PRPH2* were eligible. Genetic testing was performed using commercial providers (see Supplementary Material S1, available at www.ophthalmologyretina.org), and retinal phenotype was characterized using color, fundus autofluorescence, and OCT imaging. Only those patients who had at least 2 regions within the macular scanning area in which bands 2 and 4 could be clearly visualized were included. Pathogenicity of suspected *ABCA4* and *PRPH2* disease-causing variants was adjudicated in accordance with the guidelines set out by the American College of Medical Genetics.[19] Exclusion criteria were concomitant chorioretinal disorders confounding the diagnosis, age $<$ 12 years, and extensive macular atrophy obliterating bands 2 and 4 within the central 30° field of view. Healthy controls were individuals from our clinic without any chorioretinal disease or other ocular pathology causing reduced visual acuity (VA); they were selected by matching for age with the *ABCA4* or *PRPH2* groups during routine visits to the Lions Eye Institute.

Data Collection

Data included age, sex, genotype, phenotype, age at symptom onset, age at imaging acquisition, eye laterality (right or left) and VA using the ETDRS letter chart at the time of imaging. Phenotype grading was performed by 2 independent examiners (F.K.C. and R.H.J.) and included fleck-like retinopathy (pattern dystrophy simulating fundus flavimaculatus), central areolar choroidal dystrophy, retinitis pigmentosa, butterfly pattern dystrophy, and vitelliform macular dystrophy. Any grading disagreements were resolved by discussion. OCT scans were performed using the Heidelberg Spectralis (Heidelberg Engineering). Scanning protocols varied between study sites. OCT macula scan protocols (B-scan separation) included: 30° × 25° (60 μm), 30° × 20° (122 μm), 20° × 20° (119 μm), and 20° × 15° (245 μm). Each B-scan averaged 9 to 16 frames, and both high-speed (for eyes with poor fixation) and high-resolution (preferred for better image quality) modes were used as available. Axial resolution was 3.5 μm for the Heidelberg device.[13] One eye per patient was selected for analysis based on whichever provided the best image quality in the 4 regions of interest as determined by scrolling through volume scans. The areas with the most clearly visible outer retinal bands at the fovea as well as the superior, temporal, and inferior parafoveal regions were selected for measurement. Because *PRPH2* variants can manifest as centripetal or centrifugal atrophy, regions of outer retinal atrophy were avoided when selecting parafoveal regions for measurement, and these varied between 1000 and 3000 μm from the foveal center depending on the phenotype. In a subset of 10 eyes randomly chosen from the 45 healthy controls to reflect the mean age, bands 2 and 4 were measured at 1000, 1500, 2000, 2500, and 3000 μm from the fovea to look for variation with increasing eccentricity across different parafoveal locations. At 2500 μm temporal from the fovea, both eyes were measured to determine interocular symmetry. If the fovea was affected by atrophy, vitelliform lesion, or macular neovascularization, measurement at that specific locus was not performed. The vertical height or thickness of bands 2 and 4 was measured according to proposals by Cuenca et al[12] and the IN·OCT Consensus statement[10] by 2 independent examiners, both masked to each other's measurements but not to the diagnosis (Fig 2). All measurements were obtained using the inbuilt Heidelberg caliper function using 400% magnification. We assumed band 2 to be the EZ and the outermost hyperreflective band to be band 4 representing the RPE/Bruch complex. We noted that the structures in between these 2 bands varied considerably both between individuals and within a given scan. Some patients demonstrated a single hyporeflective gap (i.e., absence of band 3) whereas others had 1 or 2 distinct hyperreflective bands in between bands 2 and 4 (Fig 2).

Statistical Analysis

Collected quantitative data are presented in tables as mean, median, and standard deviation. In the case of qualitative variables, data are reported as percentages. Some variables are represented graphically. Patient demographics were summarized and compared among the 3 groups. Interexaminer differences in thicknesses for bands 2 and 4 were evaluated using limits of agreement and Bland−Altman plots. Interocular differences in thicknesses and

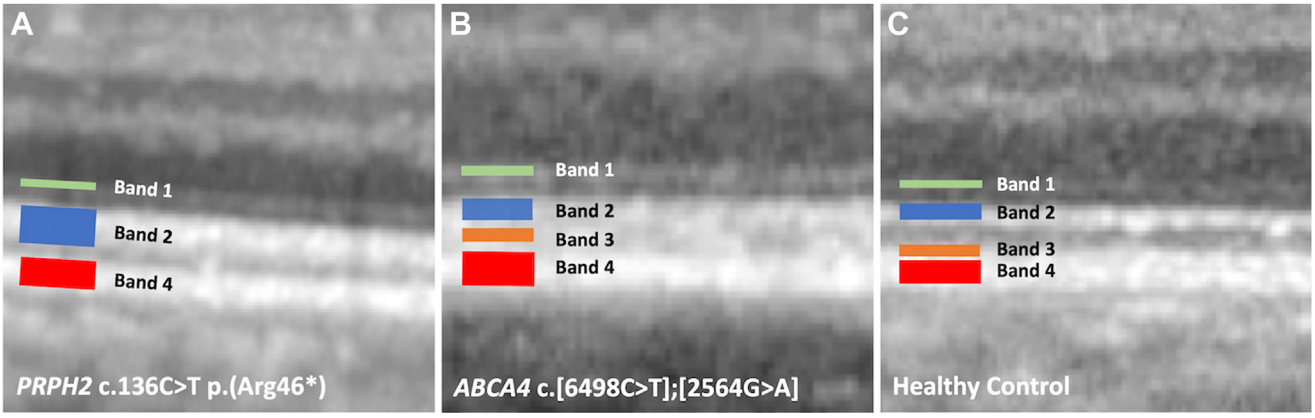

Figure 1. OCT sections of the outer retinal layers showing bands 1 to 4 in 3 examples, namely, *PRPH2*-associated retinopathy (A), *ABCA4*-associated retinopathy (B) and a healthy control (C). Note that band 3 was not visible in the patient with *PRPH2*-associated retinopathy.

ratios were assessed with a *t* test. Linear mixed modeling was used to compare the following: (1) band 2 thickness, (2) band 4 thickness, and (3) band 2/band 4 ratio across the 3 groups adjusting for age and sex. Tukey's post hoc test was used to assess pairwise differences between the groups, and estimated marginal means with 95% confidence intervals are presented. Differences in band 2 thickness, band 4 thickness, and band 2/band 4 ratio across the 5 eccentricities and 3 meridia (temporal, superior, and inferior) were assessed using linear mixed modeling, controlling for age and sex. Receiver operating characteristic (ROC) analysis was used to establish a cutoff for the thickness of bands 2 and 4 as well as the band 2/band 4 ratio, which may distinguish *PRPH2* from *ABCA4*. Model sensitivity, specificity, accuracy, and area under the curve (AUC, 95% confidence interval) were reported at the optimal cutoff. Significance was achieved if P value was < 0.05. All analyses were performed using R version 4.1.3 (R Core Team) and R Studio version 2022.07.1 (Rstudio Team).

Results

Participants

One hundred thirty-five eyes from 135 patients (45 with *PRPH2*-associated retinopathy, 45 with *ABCA4*-associated retinopathy, and 45 healthy controls) were included in the study. Each eye contributed up to 4 separate measurements (foveal, superior, temporal, and inferior parafoveal loci) for bands 2 and 4. Areas affected by outer retinal band disruption, however, were not included (Table 1). This was predominately found at the fovea and was attributed to atrophy. There was no significant difference in age across the 3 groups ($P = 0.104$). Women, however, were significantly underrepresented in the *PRPH2* group as compared with the *ABCA4* and control groups ($P = 0.013$, Table 1). The Kruskal–Wallis test found a significant difference in baseline VA between the 3 groups ($P < 0.001$) with *ABCA4* having a lower median (quartiles: Q_1, Q_3) VA (ETDRS letters) as compared with *PRPH2* (50 [40, 80] vs. 79 [71, 83]). Genotype–phenotype correlations for the *PRPH2* and *ABCA4* groups are summarized in Tables S2 and S3 (available at www.ophthalmologyretina.org). A total of 26 unique *PRPH2* variants from 34 families were found, and 7 of these were novel including 4 missense (c.515G>A, c.515G>T, c.599T>C, and c.534A>C) and 3 truncating (c.1_7delATGGCGC, c.897dupT, and c.964_965delAG) variants. There were 47 unique *ABCA4* variants from 38 families.

Thickness of Bands 2 and 4

Interobserver agreement between the 2 examiners was performed with most loci showing agreement within ± 3 μm (Supplementary Material S1). The bias of + 0.01 to + 0.50 μm (difference between examiners 1 and 2) was not statistically significant. In 10 healthy control eyes, (mean age = 56.9 years, women = 60%), there was no statistically significant difference in the thickness of bands 2 and 4 when measured at 1000, 1500, 2000, 2500, and 3000 μm from the fovea ($P > 0.05$, Supplementary Material S1). There were no statistically significant interocular differences in band 2 thickness (14.7 vs. 15.1 μm, $P = 0.31$) and band 4 thickness (18.7 vs. 19.6 μm, $P = 0.17$) at 2500 μm temporal to the fovea.

An average measurement from the 2 examiners was used for further analysis. Overall, the thickness of band 2 was significantly greater in patients with *PRPH2* variants (21.4 μm) as compared with those with *ABCA4* variants (15.9 μm) or the healthy controls (15.7 μm) for the parafoveal average (Table 4; Supplementary Material S2, available at www.ophthalmologyretina.org). Conversely, there was no significant difference in band 2 between patients with *ABCA4* variants and the healthy control group (Table 4, Fig 3A). Band 4 was significantly greater in the *ABCA4* group (27.5 μm) than both the *PRPH2* (21.7 μm) and healthy control (19.8 μm) groups for the parafoveal average ($P < 0.001$, Table 4, Supplementary Material S2). For the inferior and foveal loci, band 4 was not significantly different between the *PRPH2* group and healthy controls (Table 4, Fig 2A).

Receiver operating characteristic analysis showed the thickness of band 2 and band 4 alone were modest discriminators between the *PRPH2* and *ABCA4* groups with an AUC of 0.87 and 0.87 using a cutoff of > 18.6 μm for band 2 parafoveal average or < 26.2 μm for band 4 parafoveal average (Table 5). Figure 4 shows an improved ROC curve with band 4 as compared with band 2. See Supplementary Material S3, available at www.ophthalmologyretina.org for additional cutoff values for bands 2 and 4 at different parafoveal loci and their respective ROC curves.

Band 2/Band 4 Ratio

Interobserver agreement between the 2 examiners showed most parafoveal and foveal loci had limits of agreement of ± 16% (Supplementary Material S1). The slight bias of + 1% to + 2% was not statistically significant. Eccentricity did not influence the band 2/band 4 ratio (range: 0.8−0.9, $P > 0.05$, Supplementary Material S1). There was no statistically significant interocular difference in band 2/band 4 ratio (0.79 vs. 0.77, $P = 0.59$) at 2500 µm temporal to the fovea.

The band 2/band 4 ratio was significantly greater in the *PRPH2* group than both the *ABCA4* and healthy control groups for all parafoveal (1.00 vs. 0.59 vs. 0.80, $P < 0.001$) and foveal (0.99 vs. 0.65 vs. 0.86, $P < 0.001$) loci and for both examiners, Fig 3B, Table 4) The greatest difference in the mean band 2/band 4 ratio between the *PRPH2* and *ABCA4* groups was obtained from the superior parafoveal loci (1.00 vs. 0.54, $P < 0.001$, Supplementary Material S4, available at www.ophthalmologyretina.org).

Receiver operating characteristic analysis showed the band 2/band 4 ratio was a better discriminator between the *PRPH2* and *ABCA4* groups than band 2 or band 4 thickness alone (Table 5). Using a cutoff of > 0.79 the average parafoveal locus achieved 98% sensitivity, 100% specificity, and 99% accuracy in identifying patients with *PRPH2* variants (Fig 4C, Table 5, Supplementary Material S5, available at www.ophthalmologyretina.org). The area under the curve was 0.99 using the parafoveal average band 2/band 4 ratio as compared with only 0.87 when using the thicknesses of band 2 or band 4 alone (Fig 3C). Figure 5 illustrates distinct outer retinal band profiles in 10 cases of *PRPH2*- and *ABCA4*-associated retinopathy.

Power Analysis

A post hoc power analysis using G*Power found a total sample size of 135 (45 per group) was sufficient to detect a significant difference in the band 2/band 4 ratio between the 3 groups with a medium effect size (Cohen's f = 0.271) and small-medium effect size (Cohen's f = 0.135) at 80% power and 5% level of significance.

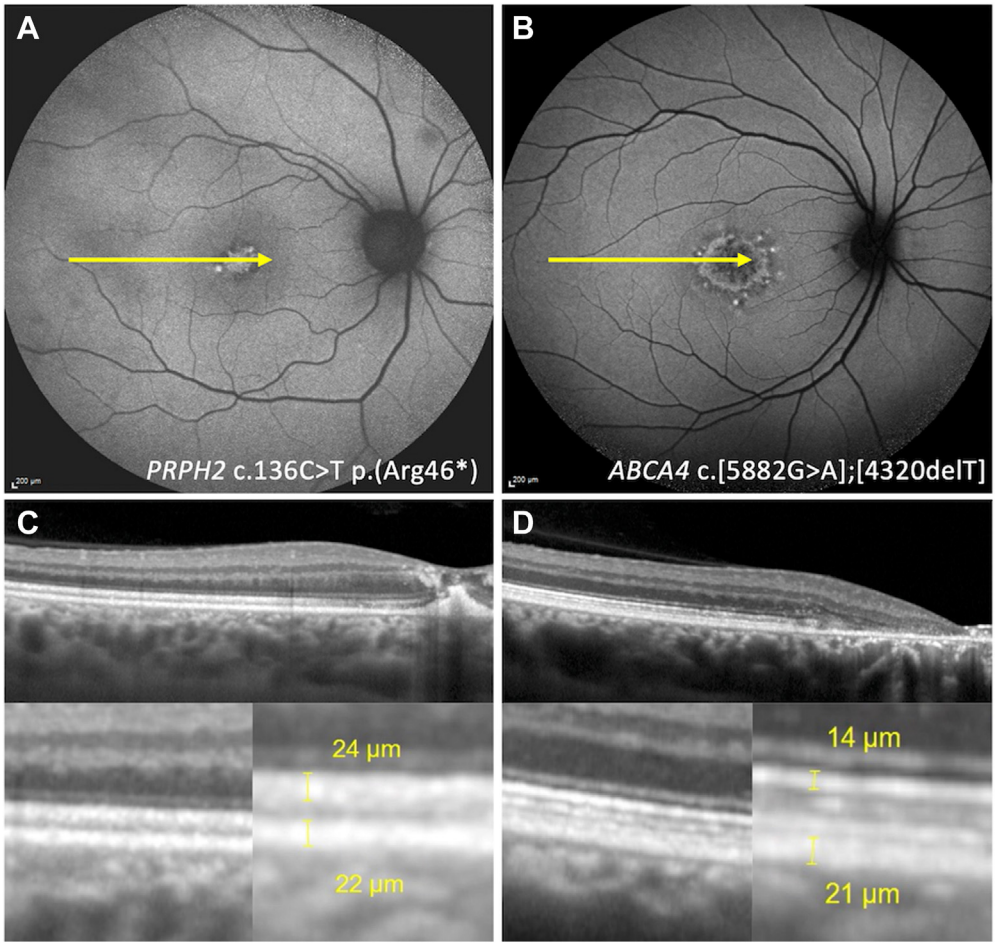

Figure 2. Fundus autofluorescence imaging showing adult-onset foveomacular vitelliform dystrophy (A) due to a heterozygous *PRPH2* mutation, and bull's-eye maculopathy (B) due to biallelic *ABCA4* mutations. Temporal OCT scans (yellow arrows) of a patient with *PRPH2*-associated retinopathy shows a foveal vitelliform lesion and an unaffected temporal retina (C). The prominent band 2 measured 24 µm compared with 22 µm for band 4. An OCT scan from a patient with *ABCA4*-associated retinopathy shows foveal outer retinal atrophy and a double hyperreflective layer in between bands 2 (14 µm) and 4 (21 µm). The duplicated band 3 was not incorporated into the band 2 or band 4 thickness measurements.

Table 1. Baseline Demographics

Variable	Level	*PRPH2*	*ABCA4*	Controls	*P*
Number of subjects		45	45	45	
Number of families		34	38	45	
Age in yrs, mean (SD)		57.4 (12.4)	50.9 (17.4)	55.6 (13.4)	0.104*
Sex	Female	16 (36%)	29 (64%)	27 (60%)	0.013†
	Male	29 (64%)	16 (36%)	18 (40%)	
Laterality	Right	40 (89%)	33 (73%)	24 (53%)	< 0.001†
	Left	5 (11%)	12 (27%)	21 (47%)	
Age of onset (yrs), median (Q_1, Q_3)		50 (43, 61)	30 (19.5, 49)	NA	< 0.001‡
VA (ETDRS letter score), median (Q_1, Q_3)		79 (71, 83)	50 (40, 80)	85 (83, 87)	< 0.001§
Number of loci with measurements	4 loci	25	19	45	
	3 loci	20	24	0	
	2 loci	0	2	0	
	1 locus	0	0	0	
Total number of loci measured by examiners		160	152	180	

ABCA4 = ATP binding cassette subfamily A member 4; NA = not applicable; Q = quartile; *PRPH2* = Peripherin-2; SD = standard deviation; VA = visual acuity.
*One-way analysis of variance
†Chi-square test
‡Mann–Whitney *U* test
§Kruskal–Wallis test

Discussion

The thickness of band 2 was significantly greater in the *PRPH2* group than the *ABCA4* and healthy control groups. Spaide and Curcio[7] found the height of the EZ among healthy controls to vary from 20 μm for the foveal cone to 16 to 17 μm for the perifoveal cone and rod photoreceptors. Our healthy control and *ABCA4* groups had a band 2 thickness of 17.0 and 17.3 μm at the fovea, respectively. This discrepancy may be related to an optical effect from light scattering properties of subcellular structures. Parafoveal band 2 thickness in controls (15.7 μm) and the *ABCA4* (15.9 μm) group was similar to histologic measurements. To our knowledge, a significantly increased height in band 2 at the fovea (20.2 μm) and parafovea (21.4 μm) with *PRPH2* mutation has not been reported. Band 2 represents the mitochondria-rich EZ,[7] and this was later supported by immunolabelling with cytochrome C.[12] In contrast, Jonnal et al[20] suggested band 2 represents the IS/OS junction using an adaptive optics OCT device. Thus, the increased height of band 2 in *PRPH2* may be due to a broadening of EZ, greater reflection at the IS/OS junction, or the fusion of bands 2 and 3. *PRPH2* is important for disc formation, stabilization, maintenance, and alignment.[21] PRPH2 forms oligomers with other PRPH2 molecules and retinal OS membrane protein 1 (ROM1).[22] Electron microscopy studies of *PRPH2* mutant mice[15] and *PRPH2* mutant human retinal tissue[16] have shown elongated, disorganized discs with compacted open discs at the base of the OS as well as swollen mitochondria in the EZ. Accumulation of light scattering subcellular structures within the IS and increased reflectivity of disorganized OS discs may contribute to the broadening of the band 2 profile. This may lead to fusion of band 2 to band 3.

The thickness of band 4 was significantly greater in the *ABCA4* group than the *PRPH2* group and healthy controls. Histology shows the height of the RPE to range from 10 to 14 μm in healthy eyes.[7] Curcio et al[23] showed the total RPE–Bruch membrane thickness was 18.8 μm in a histologic study of 18 maculae (age 40–92 years). In vivo investigations with OCT showed a much greater height of band 4: 22.7 μm[24] and 26.3 μm,[25] respectively. Given the resolution of the Heidelberg device is 3.5 μm, our results for healthy controls (20 μm) approximate published histologic estimates. However, band 4 was significantly greater in the *ABCA4* group at 27.8 μm and 27.5 μm at foveal and parafoveal regions, respectively. Band 4 was previously shown to represent RPE–Bruch complex[7] but this was later refuted by Cuenca et al[12] who suggested that both band 3 and band 4 reside within the RPE where band 4 represents the mitochondrial zone. The increased band 4 thickness in patients with variants in *ABCA4* could be because of increased height of band 4 alone, as endogenous expression of wild-type ABCA4 in the RPE may play a role in recycling retinaldehyde in the endolysosomes.[26] *ABCA4* plays an essential role in the clearance of all-*trans*-retinal.[26] Hence, lack of function results in the formation of bisretinoids in the OS discs and the RPE as lipofuscin. In an animal model of *ABCA4*, electron microscopy showed increased phagosomes with multilayered accumulation within the RPE suggesting an isolated thickening of band 4 is more likely.[17] Alternatively, the increased lipofuscin accumulation may cause a reduction in RPE melanosome density.[27,28] Cuenca et al[12] hypothesized the hyporeflective band between bands 3 and 4 is because of melanosomes. Therefore, the reduced melanosomes in patients with variants in *ABCA4* may result in loss of this hyporeflective layer and apparent fusion between bands 3

Table 4. Comparison of Bands 2 and 4, and the Band 2/Band 4 Ratio across the 3 Groups

	Locus	Mean (95% CI)			P‡
		PRPH2	ABCA4	*Controls*	
Band 2 (μm)*	Temporal	21.8 (20.8–22.9)	15.5 (14.4–16.6)§	15.6 (14.5–16.7)§	< 0.001
	Superior	21.1 (20.1–22.1)	14.9 (13.9–15.9)§	15.7 (14.8–16.7)§	< 0.001
	Inferior	21.2 (20.1–22.3)	17.2 (16.1–18.3)§	15.8 (14.8–16.9)§	< 0.001
	TSI Ave†	21.4 (20.5–22.3)	15.9 (15.0–16.8)§	15.7 (14.9–16.6)§	< 0.001
	Foveal	20.2 (19.0–21.4)	17.3 (16.0–18.7)§	17.0 (16.0–17.9)§	< 0.001
Band 4 (μm)*	Temporal	22.1 (21.0–23.2)	26.8 (25.7–27.9)	19.5 (18.4–20.6)	< 0.001
	Superior	21.4 (20.4–22.4)	28.0 (27.0–29.0)	19.7 (18.7–20.7)	< 0.001
	Inferior	21.6 (20.5–22.7)§	27.6 (26.5–28.7)	20.3 (19.2–21.4)§	< 0.001
	TSI Ave†	21.7 (20.8–22.6)	27.5 (26.6–28.3)	19.8 (19.0–20.7)	< 0.001
	Foveal	20.6 (19.4–21.8)§	27.8 (26.4–29.2)	19.9 (19.0–20.9)§	< 0.001
Band 2/Band 4 ratio*	Temporal	0.99 (0.95–1.03)	0.59 (0.55–0.63)	0.81 (0.77–0.85)	< 0.001
	Superior	1.00 (0.96–1.04)	0.54 (0.50–0.58)	0.81 (0.77–0.85)	< 0.001
	Inferior	0.99 (0.95–1.04)	0.63 (0.58–0.67)	0.79 (0.75–0.83)	< 0.001
	TSI Ave†	1.00 (0.96–1.03)	0.59 (0.56–0.62)	0.80 (0.77–0.83)	< 0.001
	Foveal	0.99 (0.95–1.04)	0.65 (0.59–0.70)	0.86 (0.82–0.89)	< 0.001

ABCA4 = ATP binding cassette subfamily A member 4; CI = confidence interval; *PRPH2* = Peripherin-2; TSI = temporal, superior, inferior.
*Average of examiners 1 and 2
†Average of temporal, superior and inferior loci
‡Thickness or ratio × group interaction
§Groups with the same superscript are not statistically significant ($P > 0.05$).

and 4. Given we observed up to 5 hyperreflective bands in *ABCA4*-associated retinopathy (Fig 1), mechanisms other than fusion may be responsible. Additional hyperreflective bands have been previously reported[13] in which one was identified along the outer portion of a serous retinal detachment. In addition, Wilk et al[29] described a fifth hyperreflective band in patients with albinism and attributed this to mitochondria in the basolateral third of the RPE cell body. In patients with variants in *ABCA4*, band 4 may be capable of segregating into 2 bands: a basal mitochondria layer and an apical lipofuscin layer. Wilson and Foster[30] and Wilson et al[31] determined that both mitochondria and lysosomes were the most important structures scattering light inside the cell.

We found that when the average parafoveal band 2/band 4 ratio was > 0.79, the patient had a *PRPH2* variant with a specificity of 100%. Previous studies examining differences between *ABCA4* and *PRPH2* expression have focused on the use of fundus autofluorescence to highlight variations in fleck morphology, distribution, peripapillary sparing, and

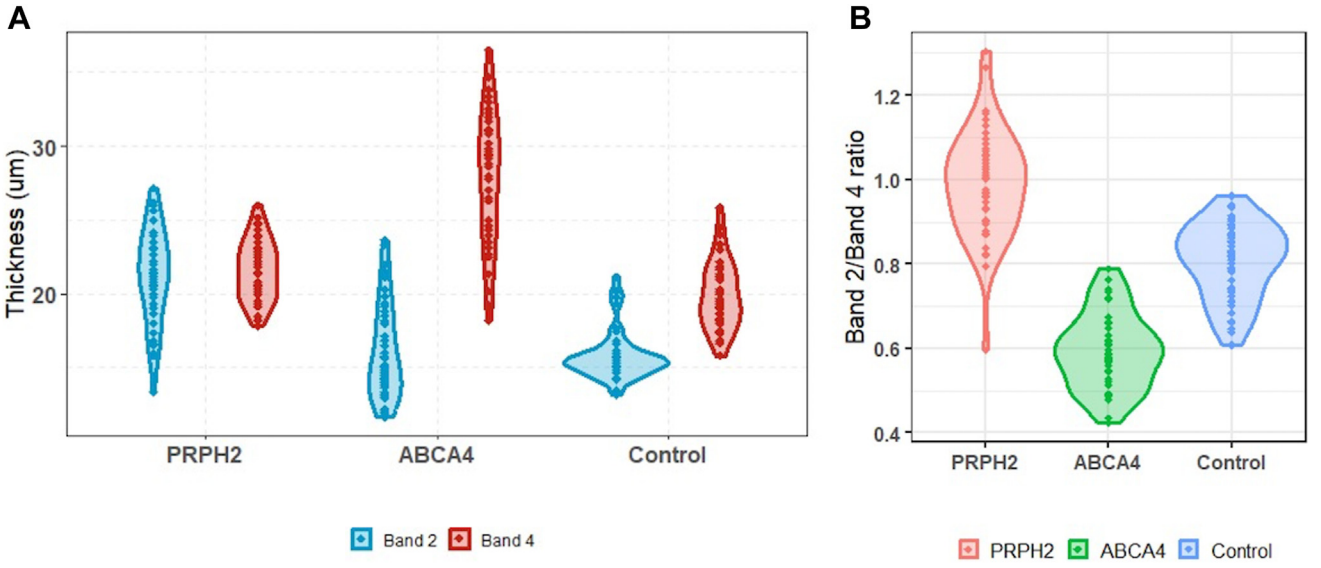

Figure 3. Violin plots showing the thickness distribution of band 2 and band 4 across the 3 groups (A). Band 2 was significantly thicker in the *PRPH2* group compared with the *ABCA4* group and controls whereas band 4 was thicker in *ABCA4* followed by *PRPH2* and controls. Band 2/band 4 ratio showed a significant difference between all 3 groups with *PRPH2* > healthy controls > *ABCA4* (B).

Table 5. Receiver Operating Characteristics Analysis of Bands 2 and 4, and the Band 2/Band 4 Ratio in Distinguishing *PRPH2* from *ABCA4*

	Locus	Optimal Thickness or Ratio Classification Rule for *PRPH2*	Specificity	Sensitivity	Accuracy	AUC (95% CI)
Band 2 (μm)*	Temporal	> 18.75	0.83	0.82	0.83	0.86 (0.77–0.86)
	Superior	> 17.25	0.82	0.84	0.83	0.91 (0.85–0.91)
	Inferior	> 16.75	0.56	0.86	0.70	0.73 (0.63–0.73)
	TSI Ave†	> 18.58	0.78	0.8	0.79	0.87 (0.79–0.87)
	Foveal	> 16.75	0.45	0.96	0.74	0.77 (0.63–0.77)
Band 4 (μm)*	Temporal	< 25.25	0.62	0.91	0.77	0.78 (0.67–0.78)
	Superior	< 26.25	0.64	0.96	0.8	0.85 (0.77–0.85)
	Inferior	< 25.75	0.71	0.93	0.82	0.85 (0.76–0.85)
	TSI Ave†	< 26.17	0.67	1.00	0.83	0.87 (0.79–0.87)
	Foveal	< 25.17	0.73	0.96	0.84	0.89 (0.81–0.89)
Band 2/Band 4 ratio*	Temporal	> 0.87	0.98	0.91	0.94	0.98 (0.95–0.98)
	Superior	> 0.73	0.98	0.93	0.96	0.99 (0.98–0.99)
	Inferior	> 0.86	0.98	0.81	0.90	0.94 (0.90–0.94)
	TSI Ave†	> 0.79	1.00	0.98	0.99	0.99 (0.97–0.99)
	Foveal	> 0.80	0.85	0.93	0.89	0.96 (0.92–0.96)

AUC = area under the receiver operating characteristic curve; CI = confidence interval; TSI Ave = temporal, superior, inferior parafoveal average.
*Average of examiners 1 and 2
†Average of temporal, superior and inferior parafoveal loci.

border features surrounding central hypoautofluorescence.[1,32] Miere et al[33] found retinal experts had an accuracy of 0.8 and sensitivity and specificity of 0.8 and 0.8, respectively, in distinguishing *ABCA4* from *PRPH2* using short-wavelength fundus autofluorescence. In contrast, retinal fellows had an accuracy of 0.7 and sensitivity and specificity of 0.6 and 0.6, respectively, whereas a deep learning classifier (ResNet50V2) identified 88/91 *ABCA4* and 10/20 *PRPH2* variants correctly with an AUC of 0.9. Using qAF, Duncker et al[6] differentiated patients with *ABCA4* mutations from a pattern dystrophy attributed to *PRPH2* or non-*PRPH2* mutations. They found qAF was not useful in differentiating *PRPH2* from *ABCA4* given the unexpectedly higher than normal qAF level in some *PRPH2* cases. Importantly, neither the ResNet50V2 nor qAF device are easily accessible to most ophthalmologists. We showed the band 2/band 4 ratio has a greater accuracy, up to 99%, for distinguishing *PRPH2*- from *ABCA4*-associated retinopathy. Our results are generalizable as we included *PRPH2* patients with a rod-cone dystrophy as well as nonpenetrant carriers. Our study also is one of the largest sample sizes of *ABCA4* vs. *PRPH2*.

This study has some limitations. First, many patients had extensive atrophy beyond the 30° × 30° imaging field, and we did not measure the nasal perifoveal region, which may have allowed more subjects to be included given *PRPH2* has a temporal predilection for RPE and outer retinal atrophy. Indeed, most patients with *ABCA4* mutations showed a macular dystrophy phenotype because those with a cone or cone-rod dystrophy typically demonstrated significant macular atrophy precluding measurement of the outer retinal bands (Table S2). Second, the resolution limits of current

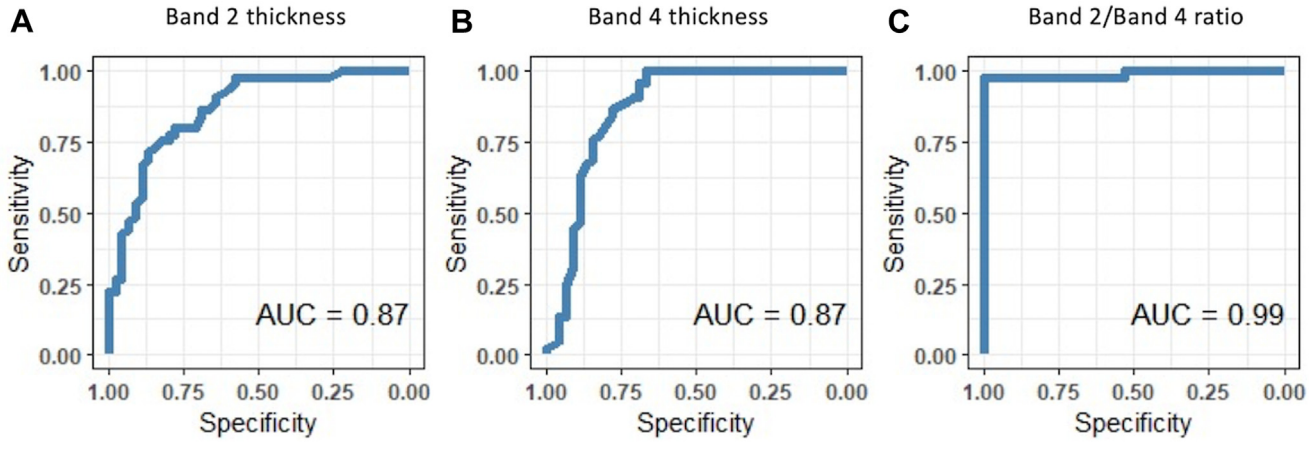

Figure 4. Receiver operating characteristic curves for the average perifoveal band 2 thickness (A), band 4 thickness (B), and band 2/band 4 ratio (C) with optimized cut off thresholds of > 18.6 μm, < 26.2 μm and > 0.8, respectively, to distinguish *PRPH2*- from *ABCA4*-associated retinopathy. AUC = area under the curve.

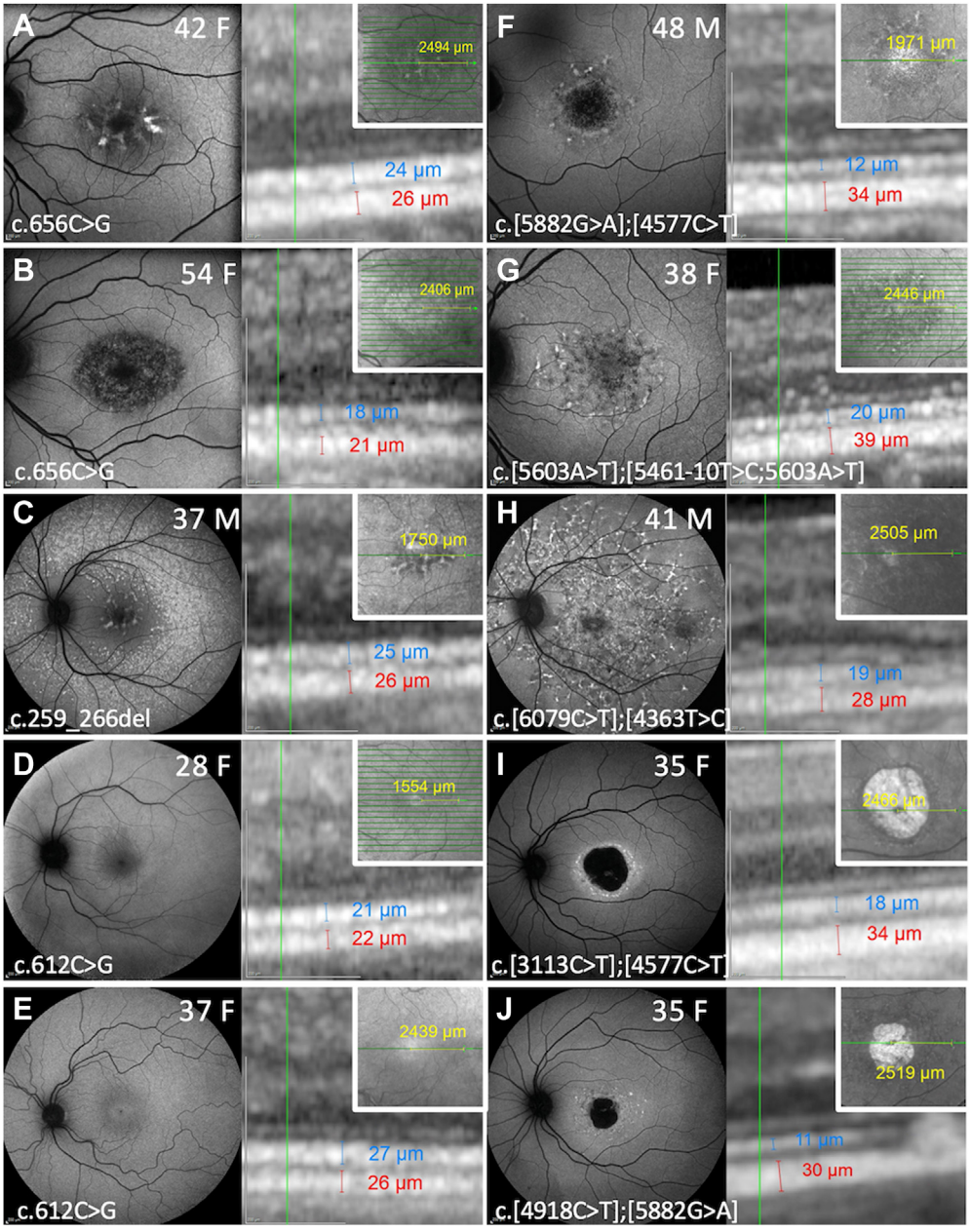

Figure 5. Examples of *PRPH2*- (A-E) and *ABCA4*-associated retinopathy (F-J) showing fundus autofluorescence imaging, genotype, age, sex, location of measurement relative to the foveal center (insert), and magnified view (400%) of the outer retinal bands. Cases A and B are siblings with butterfly pattern dystrophy (A) and central areolar choroidal dystrophy (B). Case C has pseudo-Stargardt pattern dystrophy phenotype with central flecks resembling butterfly pattern dystrophy. Cases D and E are siblings with a rod-cone dystrophy phenotype (D) and no apparent retinal disease (E). Cases F and G show localized perifoveal flecks. Case H illustrates hyperautofluorescent flecks distributed throughout the posterior pole with peripapillary sparing. Cases I and J demonstrate patches of central macular atrophy with surrounding hyperautofluorescent flecks. Yellow = distance from foveal center, Blue = thickness of band 2, Red = thickness of band 4.

OCT technology prevent measurements of bands 1 and 3 in µm resolution. In addition, band 3 was often the most difficult to distinguish and could be markedly disrupted in *ABCA4* or *PRPH2*. Band 1 was not measured, as this was the thinnest of the outer retinal bands, making any potential differences between the 3 groups difficult to elicit. Third, there may have been measurement bias; although we undertook actions to minimize this by blinding the examiners to each other's measurements, it was not possible to be masked to the diagnoses given the unique outer retinal band profile seen in each group (Fig 5). To verify our interpretations, future histologic studies are required to further our understandings of the outer retinal bands and their anatomic correlates in diseased states. However, given the rarity of these conditions and the significant morbidity after retinal

biopsy, there is a need for voluntary donations of retinal tissue from human cadavers with known IRDs. Finally, future validation and testing of the proposed cutoffs is required.

Our study demonstrated unique outer retinal band profiles in *PRPH2*- and *ABCA4*-associated retinopathy. Receiver operator characteristic analysis supports the use of a novel method, namely the band 2/band 4 ratio, for discriminating between these 2 IRDs. Further advances, such as the introduction of high-resolution OCT imaging, may better define these outer retinal bands and their anatomic correlates. Given the subjective nature of manual measurement of the thicknesses of bands 2 and 4, future development of automated methods is warranted. Thus, the integration of deep learning algorithms for segmentation of the outer retinal bands may facilitate the early prediction of IRD genotypes. International collaboration will be essential for the creation of large training data sets given the frequent concurrence of macular atrophy and flecks, which can minimize band visibility.

Footnotes and Disclosures

Originally received: April 2, 2023.
Final revision: May 9, 2023.
Accepted: May 12, 2023.
Available online: May 18, 2023. Manuscript no. ORET-D-23-00158R1.

[1] Centre for Ophthalmology and Visual Science, The University of Western Australia, Perth, Western Australia, Australia.

[2] Ocular Tissue Engineering Laboratory, Lions Eye Institute, Nedlands, Western Australia, Australia.

[3] Royal Victorian Eye and Ear Hospital, East Melbourne, Victoria, Australia.

[4] School of Science, Edith Cowan University, Perth, Western Australia, Australia.

[5] Australian Inherited Retinal Disease Registry and DNA Bank, Department of Medical Technology and Physics, Sir Charles Gairdner Hospital, Nedlands, Western Australia, Australia.

[6] Department of Optometry and Vision Sciences, University of Melbourne, Melbourne, Victoria, Australia.

[7] Centre for Eye Research Australia, Royal Victorian Eye and Ear Hospital, Melbourne, Victoria, Australia.

[8] Ophthalmology, Department of Surgery, University of Melbourne, Melbourne, Victoria, Australia.

[9] Department of Ophthalmology, FMHS, New Zealand National Eye Centre, University of Auckland, Auckland, New Zealand.

[10] Eye Department, Greenlane Clinical Centre, Auckland District Health Board, Auckland, New Zealand.

[11] Ophthalmology Department, Royal Brisbane and Women's Hospital, Herston, Queensland, Australia.

Disclosures:

All authors have completed and submitted the ICMJE disclosure form.

The authors made the following disclosures: J.A.T.: Research support − Retina Australia.

T.M.L.: Research support − Retina Australia.

T.L.M.: Research support − Retina Australia.

J.N.D.R.: Research support − Retina Australia.

L.N.A.: Research support − Novartis, Apellis, National Health & Medical Research Council of Australia (grant no: GNT#1195713).

A.S.: Research support − Novartis, Apellis, National Health & Medical Research Council of Australia (grant no: GNT#1195713).

F.K.C.: Research support − Future Health Research and Innovation Fund, the McCusker Charitable Foundation, Channel 7 Telethon Trust, Retina Australia, National Health & Medical Research Council of Australia (project and fellowship grant no.: GNT1116360, GNT1188694, GNT1054712, and MRF1142962).

The other authors have no proprietary or commercial interest in any materials discussed in this article.

HUMAN SUBJECTS: Human subjects were included in this study. The study was performed in accordance with the Declaration of Helsinki and approved by the Institutional Ethics Committees (University of Western Australia, Authorization RA/4/1/7916, RA/4/20/5454, RA/4/1/8932, and 2021/ET000151 and Sir Charles Gairdner Hospital Human Research Ethics Committee, Authorization RGS04985, the Royal Victorian Eye and Ear Hospital Human Research Ethics Committee 19/1443H, New Zealand Ministry of Health NTX/08/12/123, and Auckland District Health Board A+4290). Informed written consent was obtained from patients and controls before enrollment.

No animal subjects were used in this study.

Author Contributions:

Conception and design: Heath Jeffery, Chen

Data collection: Heath Jeffery, Thompson, Lamey, McLaren, De Roach, Ayton, Vincent, Sharma, Chen

Analysis and interpretation: Heath Jeffery, Lo, Chen

Obtained funding: Chen, Vincent, Ayton

Overall responsibility: Heath Jeffery, Lo, Thompson, McLaren, De Roach, Ayton, Vincent, Sharma, Chen.

Abbreviations and Acronyms:
ABCA4 = ATP binding cassette subfamily A member 4; **AUC** = area under the curve; **band 2** = ellipsoid zone; **band 4** = retinal pigment epithelium; **IRD** = inherited retinal disease; **IS** = inner segment; **OS** = outer segment; **PRPH2** = Peripherin-2; **qAF** = quantitative fundus autofluorescence; **ROC** = receiver operating characteristic.

Keywords:
Ellipsoid zone, Imaging biomarkers, OCT, Peripherin, Stargardt disease.

Correspondence:
Fred K. Chen, MBBS, PhD, FRANZCO, Lions Eye Institute, 2 Verdun Street, Nedlands, WA, Australia. E-mail: fred.chen@lei.org.au.

References

1. Heath Jeffery RC, Chen FK. Stargardt disease: multimodal imaging: a review. *Clin Exp Ophthalmol*. 2021;49:498−515.
2. Roshandel D, Thompson JA, Heath Jeffery RC, et al. Multimodal retinal imaging and microperimetry reveal a novel phenotype and potential trial end points in CRB1-associated retinopathies. *Trans Vis Sci Technol*. 2021;10:38.
3. Boon CJ, van Schooneveld MJ, den Hollander AI, et al. Mutations in the peripherin/RDS gene are an important cause of

multifocal pattern dystrophy simulating STGD1/fundus flavimaculatus. *Br J Ophthalmol*. 2007;91:1504−1511.
4. Michaelides M, Holder GE, Bradshaw K, et al. Cone-rod dystrophy, intrafamilial variability, and incomplete penetrance associated with the R172W mutation in the peripherin/RDS gene. *Ophthalmology*. 2005;112:1592−1598.
5. Huang D, Thompson JA, Charng J, et al. Phenotype-genotype correlations in a pseudodominant Stargardt disease pedigree due to a novel *ABCA4* deletion-insertion variant causing a splicing defect. *Mol Genet Genomic Med*. 2020;8:e1259.
6. Duncker T, Tsang SH, Woods RL, et al. Quantitative fundus autofluorescence and optical coherence tomography in PRPH2/RDS- and ABCA4-associated disease exhibiting phenotypic overlap. *Invest Ophthalmol Vis Sci*. 2015;56:3159−3170.
7. Spaide RF, Curcio CA. Anatomical correlates to the bands seen in the outer retina by optical coherence tomography: literature review and model. *Retina*. 2011;31:1609−1619.
8. Spaide RF. Questioning optical coherence tomography. *Ophthalmology*. 2012;119:2203−2204.e1.
9. Litts KM, Zhang Y, Freund KB, Curcio CA. Optical coherence tomography and histology of age-related macular degeneration support mitochondria as reflectivity sources. *Retina*. 2018;38:445−461.
10. Staurenghi G, Sadda S, Chakravarthy U, et al. Proposed lexicon for anatomic landmarks in normal posterior segment spectral-domain optical coherence tomography: the IN•OCT consensus. *Ophthalmology*. 2014;121:1572−1578.
11. Steinberg RH, Wood I, Hogan MJ. Pigment epithelial ensheathment and phagocytosis of extrafoveal cones in human retina. *Philos Trans R Soc Lond B Biol Sci*. 1977;277:459−474.
12. Cuenca N, Ortuño-Lizarán I, Pinilla I. Cellular characterization of OCT and outer retinal bands using specific immunohistochemistry markers and clinical implications. *Ophthalmology*. 2018;125:407−422.
13. Bloom SM, Singal IP. Revised classification of the optical coherence tomography outer retinal bands based on central serous chorioretinopathy analysis. *Retina*. 2021;41:181−188.
14. Charng J, Attia MS, Arunachalam S, et al. Increased interdigitation zone visibility on optical coherence tomography following systemic fibroblast growth factor receptor 1-3 tyrosine kinase inhibitor anticancer therapy. *Clin Exp Ophthalmol*. 2021;49:579−590.
15. Lewis TR, Makia MS, Kakakhel M, et al. Photoreceptor disc enclosure occurs in the absence of normal peripherin-2/rds oligomerization. *Front Cell Neurosci*. 2020;14:92.
16. Wickham L, Chen FK, Lewis GP, et al. Clinicopathological case series of four patients with inherited macular disease. *Invest Ophthalmol Vis Sci*. 2009;50:3553−3561.
17. Fang Y, Tschulakow A, Taubitz T, et al. Fundus autofluorescence, spectral-domain optical coherence tomography, and histology correlations in a Stargardt disease mouse model. *FASEB J*. 2020;34:3693−3714.
18. Britten-Jones AC, O'Hare F, Edwards TL, et al. Victorian evolution of inherited retinal diseases natural history registry (VENTURE study): rationale, methodology and initial participant characteristics. *Clin Exp Ophthalmol*. 2022;50:768−780.
19. Richards S, Aziz N, Bale S, et al. Standards and guidelines for the interpretation of sequence variants: a joint consensus recommendation of the American College of Medical Genetics and Genomics and the Association for Molecular Pathology. *Genet Med*. 2015;17:405−424.
20. Jonnal RS, Kocaoglu OP, Zawadzki RJ, et al. The cellular origins of the outer retinal bands in optical coherence tomography images. *Invest Ophthalmol Vis Sci*. 2014;55:7904−7918.
21. Chakraborty D, Strayve DG, Makia MS, et al. Novel molecular mechanisms for Prph2-associated pattern dystrophy. *FASEB J*. 2020;34:1211−1230.
22. Zulliger RZ, Conley SM, Mwoyosvi ML, et al. Oligomerization of Prph2 and Rom1 is essential for photoreceptor outer segment formation. *Hum Mol Genet*. 2018;27:3507−3518.
23. Curcio CA, Messinger JD, Sloan KR, et al. Human chorioretinal layer thicknesses measured in macula-wide, high-resolution histologic sections. *Invest Ophthalmol Vis Sci*. 2011;52:3943−3954.
24. Karampelas M, Sim DA, Keane PA, et al. Evaluation of retinal pigment epithelium−Bruch's membrane complex thickness in dry age-related macular degeneration using optical coherence tomography. *Br J Ophthalmol*. 2013;97:1256−1261.
25. Ko F, Foster PJ, Strouthidis NG, et al. Associations with retinal pigment epithelium thickness measures in a large cohort: results from the UK Biobank. *Ophthalmology*. 2017;124:105−117.
26. Lenis TL, Hu J, Ng SY, et al. Expression of *ABCA4* in the retinal pigment epithelium and its implications for Stargardt macular degeneration. *Proc Natl Acad Sci U S A*. 2018;115:E11120−E11127.
27. Pollreisz A, Neschi M, Sloan KR, et al. Atlas of human retinal pigment epithelium organelles significant for clinical imaging. *Invest Ophthalmol Vis Sci*. 2020;61:13−13.
28. Feeney L. Lipofuscin and melanin of human retinal pigment epithelium. Fluorescence, enzyme cytochemical, and ultrastructural studies. *Invest Ophthalmol Vis Sci*. 1978;17:583−600.
29. Wilk MA, McAllister JT, Cooper RF, et al. Relationship between foveal cone specialization and pit morphology in albinism. *Invest Ophthalmol Vis Sci*. 2014;55:4186−4198.
30. Wilson JD, Foster TH. Characterization of lysosomal contribution to whole-cell light scattering by organelle ablation. *J Biomed Opt*. 2007;12:030503.
31. Wilson JD, Cottrell WJ, Foster TH. Index-of-refraction-dependent subcellular light scattering observed with organelle-specific dyes. *J Biomed Opt*. 2007;12:014010.
32. Stuck MW, Conley SM, Naash MI. *PRPH2/RDS* and *ROM-1*: Historical context, current views and future considerations. *Prog Retin Eye Res*. 2016;52:47−63.
33. Miere A, Zambrowski O, Kessler A, et al. Deep learning to distinguish ABCA4-related Stargardt disease from *PRPH2*-related pseudo-Stargardt pattern dystrophy. *J Clin Med*. 2021;10:5742.